AlGaN/GaN HEMTs on Free-standing GaN Substrates with Breakdown Voltage of 5 kV and Effective Lateral Critical Field of 1 MV/cm

Jie H. Ng, Joel T. Asubar, Hirokuni Tokuda, Masaaki Kuzuhara

Graduate School of Engineering, University of Fukui, 3-9-1 Bunkyo, Fukui 910-8507, Japan
e-mail: joel@u-fukui.ac.jp, kuzuhara@fuee.u-fukui.ac.jp Phone: +81-776-9714

Keywords: AlGaN, GaN, HEMT, Breakdown, Free-standing GaN Substrate

Abstract

Three types of AlGaN/GaN HEMTs were fabricated on a free-standing GaN substrate with different depths of mesa isolation, i.e., device A with mesa surface falling on an undoped GaN channel, device B with mesa surface falling on an Fe-doped GaN buffer, and device C with mesa surface extending into a semi-insulating GaN substrate. The device with deepest mesa-etching (device C) exhibited a linear increase in the breakdown voltage without a sign of saturation up to 5 kV, indicating an effective lateral critical electric field of 1 MV/cm. It was found that the breakdown of device C was primarily determined by the resistivity of semi-insulating GaN substrate. An effective lateral breakdown electric field of 2 MV/cm was achieved from a GaN substrate with a higher doping concentration of Fe.

INTRODUCTION

Owing to its expected high critical electric field (E_{cr}) of over 3 MV/cm, GaN is predicted to play the role of key semiconductor material for realizing high-voltage and low-loss power devices [1]-[2]. However, at present, although off-state breakdown voltages of over 1 kV have been repeatedly reported in lateral AlGaN/GaN HEMTs, extracted values of effective E_{cr}, defined as the measured breakdown voltage (V_{br}) divided by the gate-to-drain spacing (L_{gd}), are typically less than 1 MV/cm [3]-[14]. This value is far below the expected maximum theoretical limit. This is partially because AlGaN/GaN HEMTs are usually fabricated on foreign substrates such as sapphire, SiC, and silicon, which tends to generate high density of threading dislocation of typically 10^8-10^{10} cm^{-2}. High density defects could be the source of leakage current paths through the buffer layer. Some of the reported values of V_{br}, L_{gd}, and corresponding effective E_{cr} measured on different substrates are as follows: 1100 V, 16 µm, and 0.69 MV/cm on sapphire [3], 1700 V, 20 µm, and 0.85 MV/cm on SiC [4], 3000 V, 40 µm, 0.75 MV/cm on Si [5], and 1370 V, 18 µm, 0.76 MV/cm on glass [6]. These results imply that free-standing GaN substrates with a nominal low dislocation density may offer an avenue of realizing improved record values in both V_{br} and E_{cr}. In order to further reduce the leakage current and thus increase breakdown voltages in AlGaN/GaN HEMTs, GaN buffer layers have been doped with impurities such as Fe [15], [16].

In this work, we present our investigation results on the relationship between V_{br} and L_{gd} of AlGaN/GaN HEMTs fabricated on a free-standing GaN substrate with different mesa isolation depths.

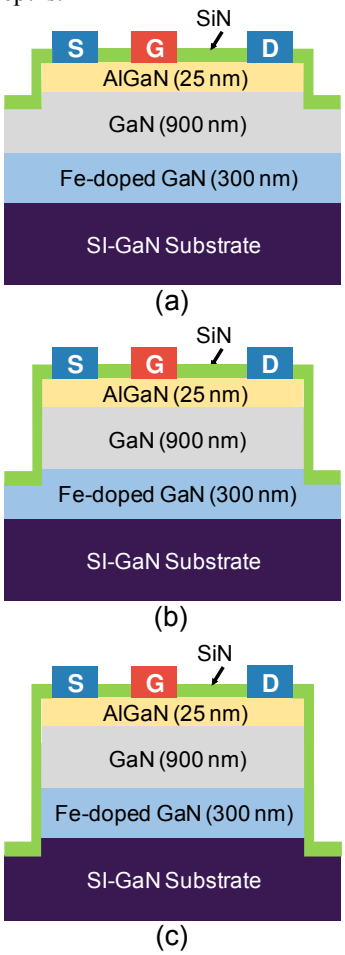

Fig. 1. Schematic cross-sectional view of three-types of AlGaN/GaN HEMTs fabricated on semi-insulating GaN substrate with different mesa depth of (a) 200 nm (device A), (b) 1000 nm (device B), and (c) 1400 nm (device C). Mesa surface falls on undoped GaN channel layer, Fe-doped GaN buffer layer, and semi-insulating GaN substrate, for devices A, B, and C, respectively.

EXPERIMENTS

All the devices were fabricated on AlGaN/GaN heterostructures grown by metal-organic chemical vapor

8b

deposition (MOCVD) on a 2-inch free-standing GaN substrate with a nominal low dislocation density of 10^6 cm^{-2}. The GaN substrate was prepared by hydride vapor phase epitaxy (HVPE) and doped with Fe with a doping concentration of about $1x10^{18}$ cm^{-3} to ensure semi-insulating property. The epitaxial structure consists of a 25 nm-thick AlGaN barrier layer with an Al composition of 0.2, a 900 nm-thick undoped GaN channel layer, and a 300 nm-thick Fe-doped GaN buffer layer. Room-temperature Hall-effect measurements revealed an electron sheet concentration of $8x10^{12}$ cm^{-2} together with a Hall mobility of 1800 $cm^2V^{-1}s^{-1}$. The device fabrication process started with the formation of mesa isolation by inductively coupled plasma reactive ion etching (ICP-RIE) using a gas mixture of BCl_3/Cl_2. Mesa isolation for device C was carried out for 170 min with BCl_3/Cl_2 (2 sccm/2 sccm), pressure of 0.25 Pa, ICP power of 20 W, and DC bias power of 20 W. For source/drain ohmic contact formation, a Ti/Al/Mo/Au (15/60/35/50 nm) metal stack was deposited, followed by rapid thermal annealing for 30 s under N_2 ambient. Nominal contact resistance was 0.4 Ωmm. After the formation of ohmic electrodes, Ni/Au (50/150 nm) was then deposited to form Schottky gates. Finally, all devices were passivated with 150 nm-thick SiN. For investigating possible leakage paths, three devices with different mesa isolation depths of 200 nm (device A), 1000 nm (device B), and 1400 nm (device C), were fabricated as illustrated in Fig. 1. For all devices, the gate-to-source spacing (L_{gs}), gate length (L_g), and gate width (W_g) were held constant at 3, 3, and 100 µm, respectively, while L_{gd} was varied from 5 to 100 µm.

RESULTS AND DISCUSSION

Figure 2 shows typical DC output and transfer characteristics of device C with gate-to-drain spacing of 10 µm. The device exhibited a maximum DC drain current density of 0.4 A/mm with a threshold voltage -2.3 V. Note that an extremely low leakage current of below 1 nA/mm was achieved, leading to an on/off ratio of more than 10^9 with a subthreshold swing (SS) of about 77 mV/dec. The maximum transconductance was typically around 125 mS/mm. Almost identical DC output and transfer characteristics were obtained from both devices A and B.

Figure 3 shows the three-terminal off-state breakdown voltage as a function of L_{gd} for three types of devices. The breakdown voltage was defined as the drain voltage at which the drain current reaches 1 mA/mm. For device A, V_{br} increased linearly with L_{gd} and reached 3.6 kV at L_{gd} = 60 µm, beyond which the device showed saturation in V_{br} at around 4 kV. From the slope in the linear region of this plot, an effective E_{cr} was calculated to be 0.6 MV/cm, which is much lower than those ever reported for devices fabricated on foreign substrates. For device B, whose surface of mesa isolation falls on the Fe-doped GaN buffer layer, V_{br} linearly increased up to L_{gd} = 60 µm and then became saturated also at around 4 kV. The overall breakdown behavior of device B was essentially the same as that of device A, indicating that the presence of 900 nm GaN channel layer in the mesa area does not induce significant additional leakage current components. Interestingly, an entirely different breakdown behavior was observed for device C, where the surface of mesa isolation falls within the bulk of semi-insulating GaN substrate. Note that device C exhibited an almost linear increase with no sign of saturation in V_{br} up to 5 kV.

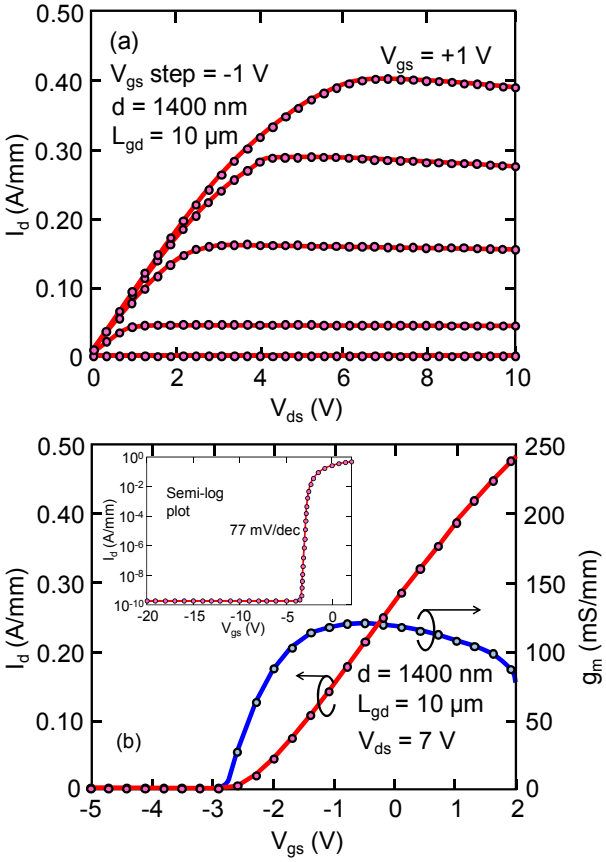

Fig. 2. (a) I_d-V_{ds} and (b) I_d-V_{gs} curves of AlGaN/GaN HEMT with mesa depth of 1400 nm and gate-to-drain spacing (L_{gd}) of 10 µm

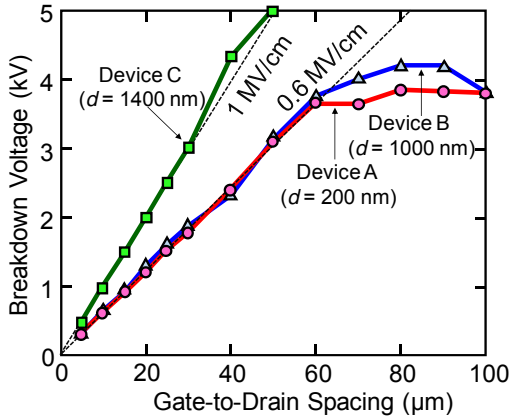

Fig. 3. Off-state breakdown voltage as a function of gate-to-drain spacing (L_{gd}) for devices with different mesa depths: device A (d = 200 nm), device B (d = 1000 nm), and device C (d = 1400 nm).

The extracted effective E_{cr} was increased to about 1 MV/cm, which is 1.7 times improvement over those of devices A and B.

Figure 4 compares the data obtained from device C to those data previously reported in literature [1, 4, 5]. To the best of our knowledge, the obtained V_{br} of 5 kV is the highest ever reported among planar AlGaN/GaN HEMTs having all electrodes formed on the front surface. Nonetheless, E_{cr} of 1 MV/cm is still far below the expected theoretical limit of 3 MV/cm, even though we were successful in increasing the effective E_{cr} by using deeper mesa isolation geometries.

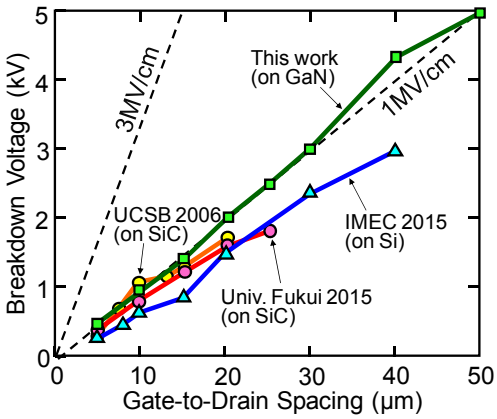

Fig. 4. Summary of off-state breakdown voltage as a function of gate-to-drain spacing (L_{gd}) for device C. Also shown are similar plot reported in references [1, 4, and 5]

It is highly probable that the leakage current through the free-standing GaN substrate still may play a significant role in limiting E_{cr}. In order for the experimental E_{cr} to approach its expected maximum theoretical value, it would be necessary to further compensate the background carrier concentration included in the semi-insulating GaN substrate by increasing Fe doping concentration. We thus investigated the breakdown characteristics of HVPE-grown GaN substrates with two different Fe concentrations, i.e., one with ~10^{18} cm^{-3} (substrate A) and the other with 9x10^{19} cm^{-3} (substrate B). Ohmic contact pairs with varying distances were directly formed on the surface of the Fe-doped GaN substrate. Figure 5 shows two-terminal breakdown voltage as a function of ohmic-to-ohmic spacing for these two GaN substrates. Substrate A showed an effective E_{cr} of 1 MV/cm, which is similar to that obtained from device C. On the other hand, substrate B exhibited an extremely high E_{cr} of 2 MV/cm. The resistivity of each GaN substrate was evaluated from the I-V characteristics measured between two ohmic contacts. It was found that the resistivity of substrate A was 6x10^{7} Ωcm, while that for sample B was over 10^{11} Ωcm. These results strongly suggest that the high resistivity of GaN substrate is the key for realizing unprecedented breakdown characteristics in lateral AlGaN/GaN HEMTs.

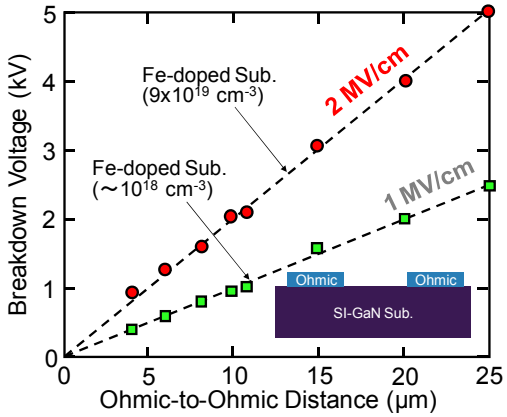

Fig. 5. Breakdown voltage as a function of ohmic-to-ohmic spacing for GaN substrates with different Fe doping concentrations.

CONCLUSIONS

We have fabricated three types of AlGaN/GaN HEMTs on a free-standing GaN substrate with different depths of mesa isolation, i.e., device A with mesa surface falling on an undoped GaN channel layer, device B with mesa surface falling on an Fe-doped GaN buffer layer, and device C with mesa surface falling on a semi-insulating GaN substrate. Breakdown voltages in device A and B were found to increase linearly up to a gate-to-drain spacing of 60 μm and then became saturated at around 4 kV. Meanwhile the breakdown voltage in device C exhibited a linear increase without a sign of saturation up to 5 kV, corresponding to an effective lateral critical electric field of 1 MV/cm. Separate measurements of breakdown electric field for the semi-insulating GaN substrate resulted in the same breakdown field of 1 MV/cm, indicating that the breakdown field of device C is primarily determined by the resistivity of semi-insulating GaN substrate. By further increasing the Fe doping concentration in the semi-insulating GaN substrate, we have succeeded in achieving an effective breakdown electric field of 2 MV/cm.

ACKNOWLEDGEMENTS

This work was partially supported by a Super Cluster Program from JST. The HVPE growth of high-resistivity GaN substrates by Prof. Kazuyuki Tadatomo, Yamaguchi University, is highly appreciated.

REFERENCES

[1] M. Kuzuhara and H. Tokuda, *IEEE Trans. Electron Devices*, vol. 62, pp. 405-413, Feb. 2015.
[2] L. F. Eastman and U. K. Mishra, *IEEE Spectrum*, pp. 28-33, May 2002.
[3] Y. C. Choi, M. Pophristic, B. Peres, M. G. Spencer, and L. F. Eastman, *J. Vac. Sci. Technol. B*, vol. 24, pp. 2601-2605, Nov./Dec. 2006.

8b

[4] Y. Dora, A. Chakraborthy, L. McCarthy, S. Keller, S. P. DenBaars, and U. K. Mishra, *IEEE Electron Device Lett*., vol. 27, no. 9, pp. 713-715, Sep. 2006.
[5] N. Herbecq, I. Roch-Jeune, A. Linge, B. Grimbert, M. Zegaoui, and F. Medjdoub, *Electron. Lett*., vol. 51, no. 19, pp. 1532-1534, Sep. 2015.
[6] B. Lu and T. Palacios, *IEEE Electron Device Lett*., vol. 31, no. 9, pp. 951-953, Sep. 2010.
[7] Q. Jiang, C. Liu, Y. Lu, and K. J. Chen, *IEEE Electron Device Lett*., vol. 34, no. 3, pp. 357-359, Mar. 2013.
[8] E. Bahat-Treidel, F. Brunner, O. Hilt, E. Cho, J. Wurfl, and G. Trankle, *IEEE Trans. Electron Devices*, vol. 57, no. 11, pp. 3050-3058, Nov. 2010.
[9] X. Liu et al., *Jpn. J. Appl. Phys*., vol. 52, no. 4S, p.04CF06, Apr. 2013.
[10] T. Nanjo et al., *IEEE Trans. Electron Devices*, vol. 60, no. 3, pp. 1046-1053, Mar. 2013.
[11] S. L. Selvaraj, A. Watanabe, A. Wakejima, T. Egawa, *IEEE Electron Device Lett*., vol. 33, no. 10, pp. 1375-1377, Oct. 2012.
[12] N. Tipirneni, A. Koudymov, V. Adivarahan, J. Yang, G. Simin, and M. A. Khan, *IEEE Electron Device Lett*., vol. 27, no. 9, pp. 716-718, Sep. 2006.
[13] Y. W. Lian, Y. S. Lin, H. C. Lu, Y. C. Huang, and S. S. H. Hsu, *IEEE Electron Device Lett*., vol. 33, no. 7, pp. 973-975, July 2012.
[14] S. C. Liu, B. Y. Chen, Y. C. Lin, T. E. Hsieh, H. C. Wang, and E. Y. Chang, *IEEE Electron Device Lett*., vol. 35, no. 10, pp. 1001-1003, Oct. 2014.
[15] S. Heikman, S. Keller, S. P. Denbaars, and U. K. Mishra, *Appl. Phys. Lett*., vol. 81, no. 3, pp. 439-441, 2002.
[16] V. Desmaris et al., *IEEE Trans. Electron Devices*, vol. 53, no. 9, pp. 2413-2417, Sep. 2006.

ACRONYMS

HEMT: High Electron Mobility Transistor
E_{cr}: Critical electric field
L_{gd}: Gate-to-drain spacing
V_{br}: Breakdown voltage
MOCVD: Metal-organic chemical vapor deposition
HVPE: Hydride vapor phase epitaxy
L_g: Gate length
L_{gs}: Gate-to-source spacing
W_g: Gate width